Heliyon 6 (2020) e03295

Contents lists available at ScienceDirect

Heliyon

journal homepage: www.cell.com/heliyon

Research article

Effect of nanoparticle concentration on coagulation rate of colloidal suspensions

G.Sh. Boltachev [a,*], M.G. Ivanov [a,b,**]

[a] Institute of Electrophysics, Ural Branch of Russian Academy of Sciences, Ekaterinburg, 620016, Amundsen str. 106, Russia
[b] G.G. Devyatykh Institute of Chemistry of High-Purity Substances, Russian Academy of Sciences, 49 Tropinin Str., Nizhny Novgorod, Russia

ARTICLE INFO

Keywords:
Materials science
Nanotechnology
Colloids
Concentrated
Suspension
Coagulation
Stochastic dynamics

ABSTRACT

Theoretically and with the help of numerical simulation the coagulation rate of nanoparticle suspensions is analyzed. Analytical expressions are proposed that describes the rate of stationary coagulation of the nanoparticles suspended in a solvent (dn_a/dt, where n_a is the particle concentration) and the characteristic coagulation time $\theta = -n_a/(dn_a/dt)$. In the contrast to traditionally used equations, the proposed expressions allow one to describe with high accuracy the rate of stationary coagulation of not only low concentrated suspensions, where the volume content of nanoparticles is $\rho \ll 1$ %, but also rather highly concentrated ones, at $\rho \sim 1$ % and more ($\rho = n_a v_a$ where v_a is a particle volume), which are relevant for most of the industrial applications. Analytical expressions are written for both three-dimensional geometry, which is relevant for real colloids, and two-dimensional geometry, which is useful to compare results of the analytical solution and numerical simulation. Computer experiments are performed in the framework of the two-dimensional method of stochastic dynamics. Satisfactory agreement of the obtained analytical expressions with the results of numerical calculations is demonstrated. The dependences of the coagulation time on the height of the interparticle energy barrier and on the suspension concentration are analyzed. It is shown that, in contrast to the obtained theoretical expressions, the traditionally used formulas overestimate the characteristic coagulation time for highly concentrated suspensions by more than an order of magnitude.

1. Introduction

Various emulsions, suspensions and colloidal solutions are intensively used in many fields [1, 2, 3, 4, 5]. Recently, an increased interest to the properties of suspensions happens due to their widespread use in the field of nanotechnology [4, 5, 6, 7, 8, 9]. One of the most important characteristics of a suspension is stability, i.e., the ability to maintain its properties, in particular, the concentration n_a of suspended particles over time. High attraction forces of nanosized particles determine the lyophobicity (instability) of their colloidal solutions [10]. From a thermodynamic point of view, coagulation of such suspensions is inevitable, over time, all of the suspended particles, trying to reduce their free surface, coagulate with the formation of large aggregates. The rate of this process is conveniently described by the characteristic coagulation time [3] or the relaxation time [10], $\theta = -n_a(dn_a/dt)^{-1}$. The time θ can vary widely. For values $\theta < 1$ second, one can speak of a strong instability of the solution, which makes its practical use nearly impossible. On the contrary, with large values θ, for example, several days or even years, we can speak of a relatively stable solution.

The theoretical solution to the simplified problem of coagulation of particles suspended in a liquid medium was given by M. Smoluchowski [11, 12]. Long-range particle interactions were not taken into account, and their coalescence (coagulation) occurred when the particle came into contact with the "sphere of influence" of another particle. In the framework of such a consideration, a result is obtained for the temporal dynamics of aggregate concentration n_a, which can be represented as:

$$n_a(t) = \frac{n_0}{1 + t/\theta}, \tag{1}$$

where n_0 is an initial concentration of aggregates (particles), and the parameter θ takes on the meaning of half-coagulation time [3], during which the particle concentration is halved

* Corresponding author.
** Corresponding author.
E-mail addresses: grey@iep.uran.ru (G.Sh. Boltachev), max@iep.uran.ru (M.G. Ivanov).

https://doi.org/10.1016/j.heliyon.2020.e03295
Received 5 December 2019; Received in revised form 20 January 2020; Accepted 22 January 2020
2405-8440/© 2020 The Authors. Published by Elsevier Ltd. This is an open access article under the CC BY-NC-ND license (http://creativecommons.org/licenses/by-nc-nd/4.0/).

$$\theta = \frac{1}{n_0 4\pi DR}, \qquad D = \frac{k_B T}{m\gamma}, \qquad \gamma = \frac{18\eta}{\rho_a d_a^2}, \tag{2}$$

R is the radius of the "sphere of influence", D is the aggregate diffusion coefficient, m is the mass, k_B is Boltzmann constant, T is the temperature. The parameter γ characterizing the dissipative properties of the liquid is determined in (2) according to the well-known Stokes formula [13] for spherical particles with diameter d_a and density ρ_a; η is the fluid viscosity. The Smoluchowski approach is widely used to describe the kinetics of coagulation of dispersed systems in the so-called diffusion mode [10, 14, 15, 16], and sometimes even applied to systems with strong interparticle interaction [10, 16, 17].

The interparticle forces between particles dispersed in aqueous media causea potential barrier that prevents the particle coalescence [1, 2, 3, 4, 5, 10]. This fact significantly changes the coagulation kinetics, and in particular, makes the use of Eq. (1) unreasonable. A theoretical approach to the consideration of coagulation of a dispersion system taking into account the interparticle potential barrier was proposed by Fuchs [18], who suggested the coagulation frequency J (the number of pair-wise connections of single particles per unit time in unit volume) [18, 19, 20] in the form:

$$J = n_a 4\pi D \Big/ \int_{d_a}^{\infty} \frac{1}{r^2} \exp\left(\frac{U(r)}{k_B T}\right) dr. \tag{3}$$

Using this equation, one can calculate the "stability ratio" of the dispersed systems [9, 19, 20, 21, 22]. In particular, in the work [21] a relation that determines the empirical dependence of the "stability ratio" on the height of the energy barrier was obtained. It is easy to verify that Eq. (3) gives the temporal dynamics of concentration $n_a(t)$ in the form (1) again, with a characteristic time $\theta \approx 1/n_0$.

In this paper, we demonstrate that the Eqs. (1), (2) and (3) are valid only for dilute systems ($n_a \to 0$) and do not allow describing computer simulation data for highly concentrated suspensions, when $\rho = n_a v_a \simeq 1$ % (v_a is the volume of a particle). In the framework of the Fuchs approach [18], we are going to write a more complete and correct equation, which will be tested according to two-dimensional modeling using the stochastic dynamics method.

2. Coagulation rate: analytical expressions for three- and two-dimensional geometries

In accordance with the original Fuchs approach [18], let us consider a particle diffusion in the potential field $U(r)$ of a selected particle:

$$\frac{\partial n}{\partial t} = \operatorname{div} \mathbf{j}, \qquad \mathbf{j} = -D\nabla n + \frac{n\mathbf{F}}{m\gamma}, \tag{4}$$

where $\mathbf{j}(r)$ is the particle flux density, $\mathbf{F}(r)$ is the interparticle interaction force,

$$\mathbf{j}^{(3D)} = \frac{dN}{dsdt}\vec{e}_r, \qquad \mathbf{j}^{(2D)} = \frac{dN}{dldt}\vec{e}_r, \qquad \mathbf{F} = -\nabla U, \tag{5}$$

$\vec{e}_r$ is the unit normal vector to either the element of the sphere ds (in 3D geometry) or the circular arc dl (in 2D geometry) around the selected particle. Hereinafter, we consider both 2D and 3D geometries at the same time, marking the corresponding values with a superscript in case of any differences. Since the problem is spherically (in 3D) or cylindrically (in 2D) symmetric, the particle concentration is $n(\mathbf{r}, t) = n(r, t)$ and it is related to the radial distribution function as $n(r, t) = n_a(t)\, g(r, t)$, where n_a is concentration of the suspension. The flux density has a non-zero radial component only, i.e., $\mathbf{j} = j\,\vec{e}_r$ and the Eq. (4) take the form:

$$\frac{\partial n^{(3D)}}{\partial t} = \frac{1}{r^2}\frac{\partial}{\partial r}\left(r^2 j\right), \qquad \frac{\partial n^{(2D)}}{\partial t} = \frac{1}{r}\frac{\partial}{\partial r}(rj), \qquad j = -D\frac{\partial n}{\partial r} - \frac{n}{m\gamma}\frac{dU}{dr}, \tag{6}$$

We consider the potential barrier preventing particle aggregation to be sufficiently high, thus we can speak about stationary conditions, i.e., $\partial n/\partial t = 0$. This allows us to write the radial dependence of the particle flux density:

$$j^{(3D)} = \frac{c_1}{r^2}, \qquad j^{(2D)} = \frac{c_1}{r}, \tag{7}$$

where c_1 is a constant. Substituting the radial dependence (7) of the flux density in the last Eq. (6), we obtain for the function $n(r)$ an ordinary differential equation, the general solution of which has the form:

$$n^{(3D)}(r) = \frac{-c_1}{D}\exp\left(-\frac{U(r)}{k_B T}\right)\int_{R_{ab}}^{r}\frac{1}{s^2}\exp\left(\frac{U(s)}{k_B T}\right)ds + c_2\exp\left(-\frac{U(r)}{k_B T}\right), \tag{8}$$

$$n^{(2D)}(r) = \frac{-c_1}{D}\exp\left(-\frac{U(r)}{k_B T}\right)\int_{R_{ab}}^{r}\frac{1}{s}\exp\left(\frac{U(s)}{k_B T}\right)ds + c_2\exp\left(-\frac{U(r)}{k_B T}\right), \tag{9}$$

where another integration constant c_2 is introduced.

Generally speaking, the parameter R_{ab} determines some arbitrary value of the radius, which in any case cannot be less than the sum of the radii of the interacting particles (or aggregates). In the terminology of [12] the parameter R_{ab} represents the radius of the "sphere of influence", on the surface of which there is an "absorption" of particles that are too close to the selected one. Due to the rapid decrease in the integrands in Eqs. (8) and (9) the exact value of R_{ab} is insignificant, and in what follows we will mean R_{ab} as the average diameter of interacting particles (aggregates), i.e., $R_{ab} = d_a$. The introduction of the "sphere of influence" allows us to formulate the first boundary condition for the function $n(r)$:

$$n(d_a) = 0, \tag{10}$$

and determine one of the integration constants. As a result, relations (8) and (9) take the form:

$$n^{(3D)}(r) = \frac{-c_1}{D}\exp\left(-\frac{U(r)}{k_B T}\right)\int_{d_a}^{r}\frac{1}{s^2}\exp\left(\frac{U(s)}{k_B T}\right)ds, \tag{11}$$

$$n^{(2D)}(r) = \frac{-c_1}{D}\exp\left(-\frac{U(r)}{k_B T}\right)\int_{d_a}^{r}\frac{1}{s}\exp\left(\frac{U(s)}{k_B T}\right)ds. \tag{12}$$

As the second boundary condition, one can require the equality of the function $n(r)$ with the given solution concentration far from the selected particle, i.e.,

$$\lim_{r\to\infty} n(r) = n_a, \tag{13}$$

that gives:

$$n^{(3D)}(r) = n_a\exp\left(-\frac{U(r)}{k_B T}\right)\int_{d_a}^{r}\frac{1}{s^2}\exp\left(\frac{U(s)}{k_B T}\right)ds \Big/ \int_{d_a}^{\infty}\frac{1}{s^2}\exp\left(\frac{U(s)}{k_B T}\right)ds. \tag{14}$$

$$n^{(2D)}(r) = n_a\exp\left(-\frac{U(r)}{k_B T}\right)\int_{d_a}^{r}\frac{1}{s}\exp\left(\frac{U(s)}{k_B T}\right)ds \Big/ \int_{d_a}^{\infty}\frac{1}{s}\exp\left(\frac{U(s)}{k_B T}\right)ds. \tag{15}$$

Here, it is worth noting that far from the selected particle the form of the radial distribution function strongly depends on many-particle perturbations (two, three, or more), which are not taken into account in the presented consideration. As a result, we can expect that solutions (14) and (15) will be sufficiently rigorous only in the limit of low concentration ($n_a \to 0$). For finite values of n_a, the function $n(r)$ must reach its

"asymptotic" value much earlier, at distances of the order of the average interparticle distance in the solution R_s, which is determined in accordance with the distribution law of the nearest neighbor [12],

$$\omega^{(3D)}(r) = 4\pi r^2 n_a \exp\left(-4\pi r^3 n_a / 3\right), \qquad \omega^{(2D)}(r) = 2\pi r\, n_a \exp\left(-\pi r^2 n_a\right). \tag{16}$$

The equation for the probability of detecting the nearest neighbor in the interval $(r, r+dr)$ for 2D geometry is obtained in exactly the same way as the equation for $\omega^{(3D)}(r)$ presented in [12]. For the average distance R_s, the distributions (16) give

$$R_s^{(3D)} = \Gamma(4/3)\left(\frac{3}{4\pi n_a}\right)^{1/3}, \qquad R_s^{(2D)} = \frac{1}{2\sqrt{n_a}}. \tag{17}$$

Now, using instead of (13) the condition

$$n(R_s) = n_a, \tag{18}$$

instead of Eqs. (14) and (15) we have:

$$n^{(3D)}(r) = n_a \exp\left(\frac{U(R_s) - U(r)}{k_B T}\right) \int_{d_a}^{r} \frac{1}{s^2} \exp\left(\frac{U(s)}{k_B T}\right) ds \Big/ \int_{d_a}^{R_s} \frac{1}{s^2} \exp\left(\frac{U(s)}{k_B T}\right) ds. \tag{19}$$

$$n^{(2D)}(r) = n_a \exp\left(\frac{U(R_s) - U(r)}{k_B T}\right) \int_{d_a}^{r} \frac{1}{s} \exp\left(\frac{U(s)}{k_B T}\right) ds \Big/ \int_{d_a}^{R_s} \frac{1}{s} \exp\left(\frac{U(s)}{k_B T}\right) ds. \tag{20}$$

It is easy to see that in the limit $R_s \to \infty$ the Eqs. (19) and (20) turn into (14), (15).

Substituting the distributions (19) or (20) into the last relation (6), for a stationary flux of particles falling in a unit of time on the "sphere of influence" J_p, we obtain:

$$J_p^{(3D)} = 4\pi r^2 j = -K^{(3D)} n_a, \quad K^{(3D)} = 4\pi D \exp\left(\frac{U(R_s)}{k_B T}\right) \Big/ \int_{d_a}^{R_s} \frac{1}{s^2} \exp\left(\frac{U(s)}{k_B T}\right) ds. \tag{21}$$

$$J_p^{(2D)} = 2\pi r j = -K^{(2D)} n_a, \quad K^{(2D)} = 2\pi D \exp\left(\frac{U(R_s)}{k_B T}\right) \Big/ \int_{d_a}^{R_s} \frac{1}{s} \exp\left(\frac{U(s)}{k_B T}\right) ds. \tag{22}$$

Now, recalling that the (central) particle that we have selected is not stationary, we have to double the diffusion coefficient to generalize the result of (21), (22) to the relative motion of the incident and absorbing particles (see [12], for example). In order to obtain a complete decrease of particles number per unit volume, the value of J_p has to be multiplied by the concentration n_a and divided by 2 in order not to take into account the merger of two particles twice. As a result we have:

$$\frac{dn_a}{dt} = -K n_a^2, \qquad \theta = \frac{1}{K n_a}, \tag{23}$$

where the coefficient K is again determined by Eqs. (21) and (22).

If we consider sufficiently diluted solutions for which the average interparticle distance R_s significantly exceeds the distance $R_{\max}$ corresponding to a potential barrier ($U(R_{\max}) = U_{\max}$), then the equations for the coefficient K are simplified. In three-dimensional geometry, we come to the traditionally used Eq. (3), and in two-dimensional to its analogue, with coefficients:

$$K^{(3D)} = 4\pi D \Big/ \int_{d_a}^{\infty} \frac{1}{s^2} \exp\left(\frac{U(s)}{k_B T}\right) ds, \quad K^{(2D)} = 2\pi D \Big/ \int_{d_a}^{\infty} \frac{1}{s} \exp\left(\frac{U(s)}{k_B T}\right) ds. \tag{24}$$

Otherwise, if we restrict our consideration to solutions for which $U_{\max} \gg k_B T$, we can approximate the potential energy $U(r)$ in integrals (21), (22) by the equation [18]:

$$U(r) \cong U_{\max} - m\omega^2 \frac{(r - R_{\max})^2}{2}, \tag{25}$$

and write for the coefficient K the relations:

$$K^{(3D)} = \sqrt{\frac{2}{\pi}}\, \frac{\omega}{\gamma} R_{\max}^2 v_T \exp\left(\frac{U(R_s) - U_{\max}}{k_B T}\right), \qquad v_T = \sqrt{\frac{k_B T}{m}}, \tag{26}$$

$$K^{(2D)} = \sqrt{2\pi}\, \frac{\omega}{\gamma} R_{\max} v_T \exp\left(\frac{U(R_s) - U_{\max}}{k_B T}\right), \tag{27}$$

where v_T is the average thermal velocity of suspended particles. The latter relations can be considered as a generalization of the overdamped limit of Kramers [18, 23], describing the flow of particles through a one-dimensional barrier between two potential wells of different depths.

The independence of the coefficient K from the solution concentration, observed in the framework of approximations (24), makes it easy to integrate Eq. (23), eventually resulting in the classical Eq. (1) with the corresponding parameters θ. In the general case of Eqs. (21) and (22) and in the framework of approximations (26), (27), i.e., for solutions that cannot be called dilute, the coefficient K, in view of the dependence on the value of R_s, should strongly depend on the concentration n_a. In this case, of course, the result (1) ceases to be valid.

3. Numerical simulation technique

Numerically, the problem of coagulation of a colloidal solution of nanosized particles is modeled in the framework of the two-dimensional method of stochastic dynamics [17, 24, 25, 26, 27, 28, 29, 30]. An ensemble of nanoparticles suspended in a liquid is considered. The model cell is a square in the *Oxy* plane; periodic boundary conditions apply at the boundaries. The number of particles inside the model cell is $N_p = 2500$. Particles have a perfectly spherical shape with a diameter $d_a = 10$ nm. Particle material is aluminum oxide with the density $\rho_a = 3970$ kg/m^3 [31]. Dispersion medium is water with the dielectric constant $\varepsilon_r = 80$ at the temperature of 20 °C. To estimate the viscosity η of water, the data [31] on its temperature dependence in the range of 273–400 K are approximated by the function:

$$\ln(\eta/\eta_r) = \eta_0 + \eta_1 (T/T_r) + \eta_2 (T/T_r)^2 + \eta_3 (T/T_r)^3, \tag{28}$$

where $\eta_r = 1.0$ mPa·s, $T_r = 300$ K, $\eta_0 = 34.75$, $\eta_1 = -77.40$, $\eta_2 = 56.93$, $\eta_3 = -14.46$.

Particle motion is described by the Langevin equation [24]:

$$m\frac{d\vec{v}}{dt} = \sum_j \vec{f}_{ij} - m\gamma\vec{v} + \vec{g}, \tag{29}$$

where $\vec{v}$ is the velocity of the particle i, $\vec{f}_{ij}$ is the interparticle force between the particles i and j, $\vec{g}$ is the fluid random force. To solve the stochastic Eq. (29) numerically, the corrected numerical scheme of [25] is used in the form suggested in [32]:

$$\begin{aligned} \vec{v}(t + h_t/2) &= \alpha\left(\vec{v}(t - h_t/2) + \frac{\vec{F}}{m} h_t\right) + v_T\sqrt{1-\alpha^2}\ \vec{r}^{\,G}, \\ \vec{r}(t + h_t) &= \vec{r}(t) + \vec{v}(t + h_t/2) h_t\,, \end{aligned} \tag{30}$$

where h_t is the integration step, $\alpha = \exp(-\gamma h_t)$, $\vec{r}^{\,G}$ is the "Gaussian noise" with parameters $\mu^G = 0$ and $\sigma^G = 1$. The first equation of the system (30) is an exact solution of the Langevin Eq. (29) for the velocity [12, 28].

Interparticle interactions f_{ij} include dispersion attraction (force f_a, energy U_a) and electrostatic repulsion (force f_e, energy U_e). The energy of dispersion attraction, neglecting the retardation, has a form described in [33, 34]:

$$U_a = \frac{-A}{12}\left\{\frac{d_a^2}{r^2 - d_a^2} + \frac{d_a^2}{r^2} + 2\ln\left(1 - \frac{d_a^2}{r^2}\right)\right\}, \qquad f_a = -\frac{dU_a}{dr}, \tag{31}$$

where $A = 4\pi^2\varepsilon$ is Hamaker's constant, ε is the energy parameter of the intermolecular potential. When the retardation is taken into account, the equation for the energy of dispersion attraction has a much more cumbersome form [35], which creates certain inconveniences for analytical differentiation and for use in calculations. To avoid these inconveniences and increase the speed of calculations we tabulated the force of dispersion attraction $f_a(r)$ within an interval $h_g \le r - d_a \le h_g + 2L_a$, where h_g is the minimal gap between particles (reaching the gap the particles coagulate), L_a is the characteristic retardation length. At large distances, the force f_a reaches asymptotic f_{ass}:

$$f_{ass}\frac{12L_a}{-A} = \left[y\frac{2 - 5y - 8y^2 + 3y^3}{(1-y)^3} + 2\ln(1-y)\right]\frac{x}{5} + \frac{105 - 63y + 27y^2 - 5y^3}{70(1-y)^5}y^3x^2, \tag{32}$$

where $x = L_a^2/r^2$, $y = d_a^2/r^2$. The transition to the asymptotic (32) is controlled by the parameter p_{ass}:

$$f_a(r) = f_{ass}(1 + p_{ass}x), \tag{33}$$

which is determined by the condition for matching functions $f_a(r)$ and $f_{ass}(r)$ at the point $r = d_a + h_g + 2L_a$.

To describe the electrostatic interaction of the particles due to the formation of double electric layers [2, 36, 37], the Deryagin's formula [37] was used, which gives:

$$U_e = \pi\varepsilon_0\varepsilon_r\Psi^2\frac{d_a^2}{r}\exp\left(-\frac{r - d_a}{R_D}\right), \qquad f_e = -\frac{dU_e}{dr}, \tag{34}$$

where R_D is the Debye radius, ε_0 is the electric constant, Ψ is the potential of the diffuse part of the double electric layer, taken equal to the ζ potential [27]. The applicability of the Eq. (34) is limited by the condition of a small particle charge: $\nu_i^{\pm}\Psi \ll 25$ mV, where $\nu_i^{\pm}$ is a valence of ions in the solution. This condition is often not satisfied for real suspensions [38, 39, 40, 41]. However, according to the analysis performed in [32], violation of this condition weakly affects the spatial distribution of the potential, which indicates a rather wide range of applicability of the relations (34). The values used in further calculations for all parameters included in relations (31)–(34) are presented in the Table 1.

Figure 1 shows the ratio of the maximum energies of dispersion and electrostatic interactions to the energy of thermal fluctuations. Over the entire range of particle sizes, the energy of dispersion attraction, achieved by direct contact, is several orders of magnitude higher than the energy of electrostatic repulsion and the level (k_BT) of thermal fluctuations in the system. Thus, the approach of particles to direct contact leads to their irreversible aggregation. Figure 1 also shows gravitational energy corresponding to the displacement of a particle by its diameter. It can be seen that taking in account the gravitational forces becomes necessary for particles with a diameter of more than 1 μm.

Table 1. Parameters of the particles interaction.

Parameter	Value
ε	272 k_B
L_a	50 nm
d_g	10 nm
h_a	0.1 nm
R_D	400 nm
ε_r	80
Ψ	50 mV
ρ_m	3970 kg/m^3

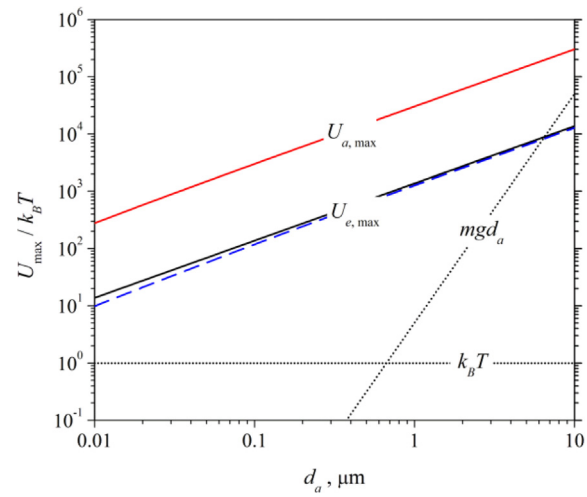

Figure 1. The maximum values of the energy of dispersion attraction $U_a$and electrostatic repulsion U_e(solid lines) achieved by contact of particles $r_{ij} = d_a + h_g$, depending on their diameter. The dashed line is the height of the energy barrier; dotted lines show levels of gravitational forces and thermal fluctuations; ζ-potential is 50 mV.

The approach of the particles is counteracted by the forces of electrostatic repulsion, which at distances of $r > 1$ nm become dominant due to a sharp decrease in the attraction forces. As a result, a potential barrier is formed (see Figure 2). At ζ-potential of 50 mV for particles with a size of $d_a = 10$ nm, the height of the potential barrier preventing particle aggregation is about 10 k_BT. This is not enough for the long-term stability of the solution. Thus, it can be expected that particles with a size $d_a = 10$ nm will gradually aggregate.

Figure 2 shows why, in addition to energy parameters, the stability of a suspension depends on the concentration of suspended particles. If the concentration of a relatively stable suspension of particles increases and, accordingly, the average distance R_s between particles decreases to values of the order of R_{max}, then the suspension ceases to be stable. The particles aggregate, since the distances which correspond to the energy barrier already overcome.

4. Numerical results and discussion

As a comparison and verification of theoretical expressions (14)–(27) and calculation programs, a stationary coagulation process in the system with a particle size $d_a = 10$ nm and a relative volume density $\rho = n_a v_a = 0.7$ % has been simulated; here $v_a = \pi d_a^3/6$ is a particle volume. To meet the stationarity condition $n_a =$ const at the instant of aggregate formation, i.e., when two particles stick together, one of the particles is supposed to be fixed and the second one to moved randomly in the free space of the solution at a sufficient distance ($\Delta r = 6d_a$) from the other particles. The same value Δr was taken as a minimal interparticle distance when an initial random configuration was generated.

Figure 3 shows a radial distribution function of the nanoparticles: $g(r) = n(r)/n_a$. The initial distribution is determined by the condition for generating the initial structures and is averaged out 300 independent generations. Settling at a stationary distribution occurs in about 5 μs. The stationary distribution curve is constructed by averaging out 300 distributions, which are taken with a time interval of about 2 μs. The figure shows, on the example of 2D geometry, that Eqs. (19) and (20) correctly reproduce the form of the function $g(r)$ in the vicinity of the energy

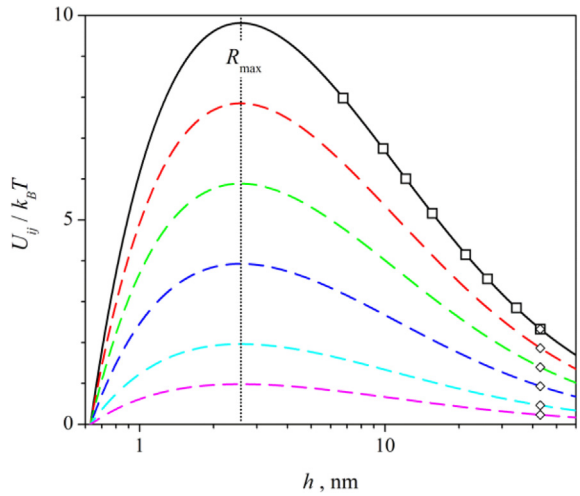

Figure 2. The interaction energy depending on the distance between particles $h = r - d_a$for particles with a diameter of 10 nm and a ζ-potential of 50 mV (solid line). Dashed lines correspond to reduced interactions by a factor of $\Upsilon =$ 0.8, 0.6, 0.4, 0.2, and 0.1. The symbols show the mean interparticle distances $R_s$in the simulated systems.

barrier at $r = R_{\max} = 1.26d_a$. For the sake of comparison, the function $g(r)$ defined by Eq. (15) is also shown there. Quite an accurate reproducibility of the pair density of particles in the vicinity $r = R_{\max}$ allows us to believe the transition rate of particles through the energy maximum to be correctly determined, and therefore, the coagulation rate in the system to be accurately estimated according to equations (21) – (23).

For a more reliable verification of the correctness of these equations, we have varied the height of the potential barrier in the model system. In order to analyze the effect of the height of the energy barrier of interparticle interactions on the rate of stationary coagulation, all interparticle forces were reduced by a factor Υ. In addition to the initial system ($\Upsilon =$ 1.0), calculations have been performed for values $\Upsilon =$ 0.8, 0.6, 0.4, 0.2, 0.1. A reduction of the potential barrier for the systems to model was shown in Figure 2. The resulting values of the characteristic coagulation time $\theta = -n_a(dn_a/dt)^{-1}$ are shown in Figure 4 depending on the height of the energy barrier. The figure proves the Eqs. (21) and (22) to accurately reproduce the dependence of the characteristic coagulation time on the height of the energy barrier. So, for the initial system ($\Upsilon = 1.0$), the calculated value is $\theta \cong 22$ ms, and the theoretical result is $\theta \cong 19$ ms. At the same time, the use of the traditional approach, i.e., of the Eq. (24), overestimates the coagulation time θ by about an order of magnitude. Here, one can note a rather high accuracy of the simplified Eq. (27). For the initial system at $\Upsilon = 1.0$ they give a somewhat underestimated result $\theta \cong 16$ ms, but with an increase in the barrier height the deviation from the result calculated in accordance with the more accurate Eq. (22) rapidly decreases (see inset in Figure 4).

To analyze an effect of nanoparticle concentration on their coagulation rate, the systems have been simulated with a volume content of the nanoparticles ρ from 0.7% to 7%, which corresponds to a decrease in the ratio R_s/d_a from 5.3 to 1.7. The results of numerical modeling are compared with the theoretical expressions (described in section 2) in Figure 5. The figure shows that at densities $\rho < 3\%$, Eqs. (22) and (27) are in a satisfactory agreement with the data of the numerical experiments. An increase in density, when $\rho > 3\%$, leads to noticeable discrepancies, which is associated with excessive convergence of the average interparticle distance R_s and the coordinate of the energy barrier $R_{\max} \cong 1.26d_a$. So, for the system with density $\rho = 7\%$, the interaction energy of particles at a distance R_s is $U(R_s) \cong 8.0k_BT$, which is not much lower than the height of the barrier $U_{\max} \cong 9.8k_BT$. At $\rho = 3\%$ the energy $U(R_s) \cong 5.2k_BT$. Thus, it can be asserted that a satisfactory agreement between the simulation data and the theoretical expressions (22) and (27) is observed when the energy $U(R_s)$ drops about half (or more) from its maximum value. To describe the simulation data in Figure 5 an empirical correction has been used:

$$\theta = \theta_{th}\left(1 + p_1\rho + (p_2\rho)^2\right), \tag{35}$$

where θ_{th} is the coagulation time determined by the theoretical expressions (22), $p_1 = 9.1$ and $p_2 = 22$. In the region of dilute solutions, at $\rho < 0.1\%$, the theoretical curves quickly approach the result corresponding to the traditional approximation (24) and coincide with it when $\rho \to 0$. However, in the high concentrations region, the traditional approximation is absolutely not applicable. For example, at $\rho = 1\%$ the estimated coagulation time is $\theta \cong 7$ ms, while the use of Eq. (24) overestimates this value by more than an order of magnitude (up to 120 ms).

Figure 6 represents a much more stable system with the parameters $d_a = 100$ nm and $\zeta = 25$ mV. The height of the energy barrier in this system $U_{\max} \cong 27k_BT$, which gives at the same concentrations approximately 7 orders of magnitude higher coagulation times than in the system

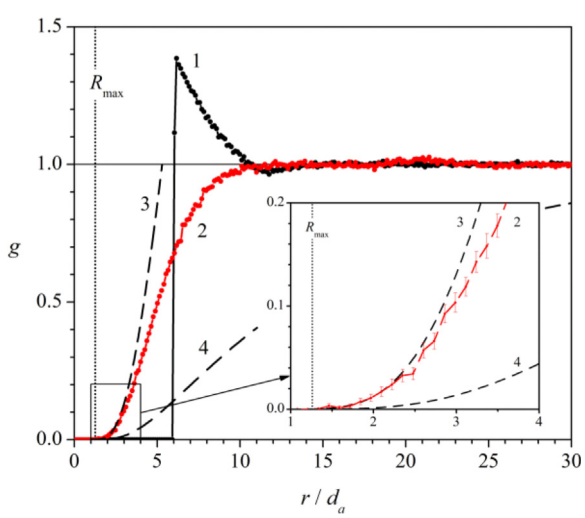

Figure 3. Radial distribution function $g(r) = n(r)/n_a$of the nanoparticles. Curve 1 is the initial particle distribution; curve 2 is the stationary distribution, which is set at $t > 5$ μs. Dashed lines correspond to the theoretical expressions of (15) (line 4) and (20) (line 3). Inset: the region near the energy maximum ($r = R_{\max}$) on an enlarged scale.

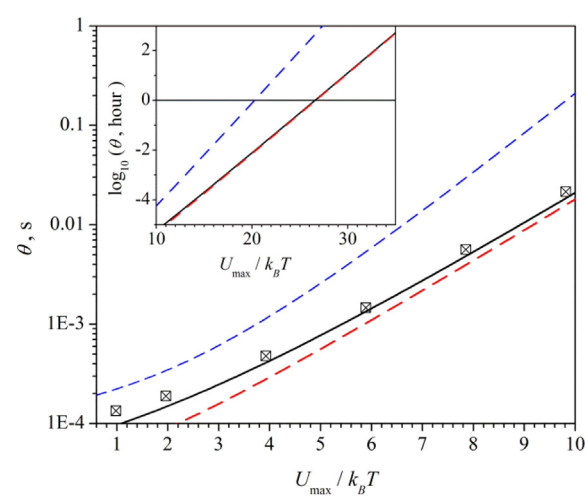

Figure 4. Coagulation time for stationary conditions depending on the height of the energy barrier. Symbols are the results of numerical simulations. Lines correspond to the theoretical Eq. (22) (solid line), (27) (bottom dashed line) and (24) (top dashed line). Inset: continuation of theoretical curves to the region of high energy barriers.

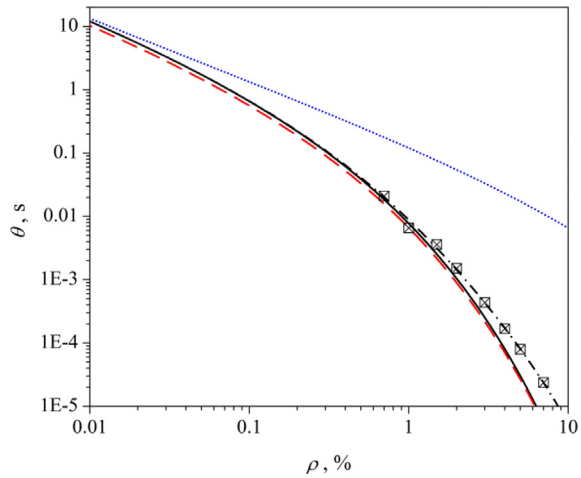

Figure 5. Dependence of coagulation time on the volume content of nanoparticles. Symbols are the numerical simulation data, lines correspond to the Eq. (22) (solid line), (27) (dashed line, red), (24) (dotted line, blue) and (35) (dashed-dotted line).

shown in Figure 5. The numerical simulation of the coagulation in such a system is quite difficult, since it is necessary to "monitor" the system for too long. Therefore, Figure 6 represents only the results of theoretical analysis. It can be seen that the large height of the energy barrier makes the difference between relations (21), (22) and approximations (26), (27) even more invisible. In this case the error in the traditional relations (24) increases much faster with increasing concentration of the solution. If the solution at $\rho = 0.1\%$ can be considered as a diluted one and the Eq. (24) can be used, then already at $\rho = 1\%$ these equations overestimate the coagulation time by 27 times: the relation (22) give $\theta \cong 1.4$ years here, and the relation (24) give $\theta \cong 37$ years.

Figure 7 represents the temporal dynamics of the structure of the solution with parameters $d_a = 10$ nm, $\zeta = 50$ mV and the volume content of the suspended particles $\rho = 7\%$. These data have been obtained by a method different from the stationary conditions used to calculate the data presented in Figures 3, 4, 5, and 6. In the calculations shown in Figure 7, we did not artificially fix the concentration of particles, but simulated a situation as close as possible to real conditions. As a result, by the end of the simulation time (slightly more than 100 μs), a noticeable fraction of binary aggregates formed in the solution, i.e., consisting of two particles, triple aggregates, quaternary ($n_4 \cong 4.3/\mu m^2$), and even one

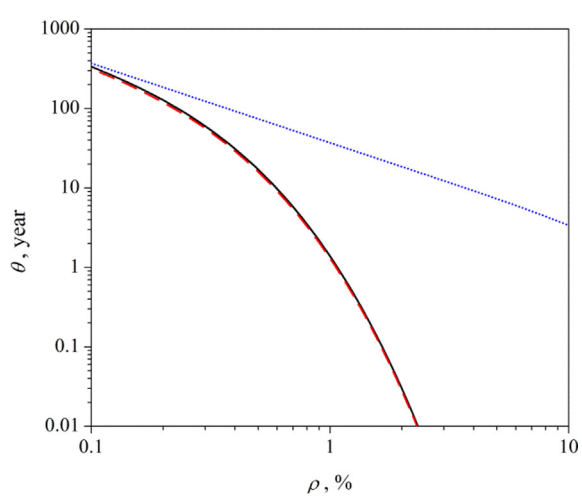

Figure 6. Dependence of coagulation time on the volume content of nanoparticles for the system: $d_a = 100$ nm, $\zeta = 25$ mV. The designations are the same as in Figure 5.

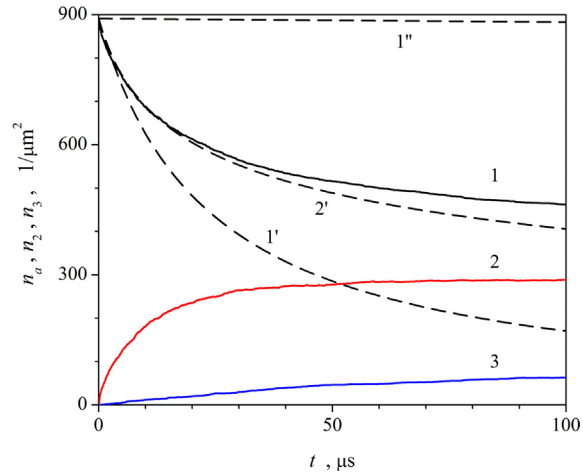

Figure 7. Temporal dynamics of aggregate concentrations in the solution. Solid lines are the numerical simulation data on the total aggregates number (line 1), binary aggregates, i.e., consisting of two particles (line 2), and triple aggregates (line 3). Dashed lines correspond to the theoretical dependences of the total aggregates number in accordance: with Eq. (1) at $\theta = 23.6$μs (line 1′), $\theta = 11$ ms (line 1″); with Eqs. (22), (23), and (35) (line 2′).

aggregate of five particles ($n_5 \cong 0.36/\mu m^2$). In the framework of traditional theoretical approach, i.e., by Eqs. (1), (23), and (24), we have $\theta = 11$ ms and the dependence $n_a(t)$, which is not consistent with simulation results (see line 1″). As noted in Section 2, the dependence of the coefficient K, which in accordance with the Eq. (23) determines the coagulation rate, on the concentration of suspended particles makes the Smoluchowski law (1) inapplicable. As can be seen in Figure 7, the curve corresponding to this law, even with an exact initial value $\theta = 23.6$ μs corresponding to Eq. (22), deviates strongly from the results of the numerical simulation (see line 1′). Consideration of the influence of concentration in the Eqs. (22), (23), and (35) allows one to reproduce the simulation data much better, although not absolutely accurately (see line 2′). For a more rigorous description of the temporal dynamics of a solution, it is necessary to take into account factors such as the fractality of growing aggregates [9, 26], changes in the height of the potential barrier [22], etc. Comparison of Figures 5 and 6, in particular, shows a sharp increase in the barrier $U_{\max}/k_BT$ with an increase in aggregate size. However, these issues are beyond the scope of the present study.

5. Conclusion

As a result of the study, analytical expressions are proposed that determine the coagulation rate of nanoparticles suspended in a solvent dn_a/dt, where n_a is the nanoparticles concentration, and the characteristic coagulation time $\theta = -n_a/(dn_a/dt)$. In contrast to the traditionally used ratios, the obtained equations allow one to describe with high accuracy the rate of stationary coagulation of not only low concentrated suspensions, when the volume content of nanoparticles $\rho \ll 1\%$, but also rather highly concentrated ones, at $\rho \sim 1\%$ and higher ($\rho = n_a v_a$, where v_a is the volume of a particle). Analytical expressions have been written for cases of three-dimensional geometry ($v_a = \pi d_a^3/6$), which is relevant for working with real nanoscale colloidal solutions, and two-dimensional geometry ($v_a = \pi d_a^2/4$), which is convenient for comparison with the corresponding results of numerical simulation. Computer experiments have been performed in the framework of the two-dimensional method of stochastic dynamics. Satisfactory agreement of the obtained theoretical expressions with the results of numerical calculations has been demonstrated. The dependences of the coagulation time on the height of the interparticle energy barrier $\theta(U_{\max}/k_BT)$ and on the volume content of the suspended particles $\theta(\rho)$ have been studied. It has been shown that, in contrast to the obtained theoretical expressions, the traditionally used

ratios for highly concentrated suspensions ($\rho \sim 1$ %) overestimate the characteristic coagulation times by more than an order of magnitude.

Declarations

Author contribution statement

Grey S. Boltachev: Conceived and designed the experiments; Performed the experiments; Analyzed and interpreted the data; Contributed reagents, materials, analysis tools or data; Wrote the paper.

Maxim G. Ivanov: Conceived and designed the experiments; Contributed reagents, materials, analysis tools or data; Wrote the paper.

Funding statement

This work was supported by Russian Science Foundation (research project No. 18-13-00355).

Competing interest statement

The authors declare no conflict of interest.

Additional information

No additional information is available for this paper.

References

[1] H.R. Kruyt (Ed.), Colloid Science. V. I. Irreversible Systems, Elsevier, Amsterdam, 1952.
[2] S.S. Dukhin, B.V. Deryagin, Electrophoresis, Nauka, Moscow, 1976 [In Russian].
[3] A.D. Zimon, Colloid Chemistry (Including Nanopaticles): Textbook, Agar, Moscow, 2007 [In Russian].
[4] B. Gilbert, G. Lu, C.S. Kim, Stable cluster formation in aqueous suspensions of iron oxyhydroxide nanoparticles, J. Colloid Interface Sci. 313 (2007) 152–159.
[5] M.-L. Rami, M. Meireles, B. Cabane, C. Guizard, Colloidal stability for concentrated Zirconia aqueous suspensions, J. Am. Ceram. Soc. 92 (s1) (2009) S50–S56. Special Issue: Ceramic Processing Science.
[6] I. Corni, M.P. Ryan, A.R. Boccaccini, Electrophoretic deposition: from traditional ceramics to nanotechnology, J. Eur. Ceram. Soc. 28 (2008) 1353–1367.
[7] S. Dor, S. Rühle, A. Ofir, M. Adler, L. Grinis, A. Zaban, The Influence of Suspension Composition and Deposition Mode on the Electrophoretic Deposition of TiO_2 Nanoparticle Agglomerates, Colloids Surface. A Physicochem. Eng. Aspects 342 (2009) 70–75.
[8] S. Radice, C.R. Bradbury, J. Michler, S. Mischler, Critical particle concentration in electrophoretic deposition, J. Eur. Ceram. Soc. 30 (2010) 1079–1088.
[9] C.O. Metin, R.T. Bonnecaze, L.W. Lake, C.R. Miranda, Q.P. Nguyen, Aggregation kinetics and shear rheology of aqueous silica suspensions, Appl. Nanosci. 4 (2) (2014) 169–178.
[10] C. Cametti, P. Codastefano, P. Tartaglia, Light-scattering measurements of slow aggregation in colloids: deviations from asymptotic time scaling, Phys. Rev. A. 36 (10) (1987) 4916–4921.
[11] M.V. Smoluchowski, Brownsche Molekularbewegung und Koagulation von Kolloidteilchen, Phys. Zeits. 17 (1916) 557–571, 585-599.
[12] S. Chandrasekhar, Stochastic problems in physics and astronomy, Rev. Mod. Phys. 15 (1943) 1–89.
[13] L.D. Landau, E.M. Lifshitz, Course of theoretical physics, in: Fluid Mechanics, 2nd. ed. 6, Pergamon, Oxford, 1987.
[14] M. Kolb, Unified description of static and dynamic scaling for kinetic cluster formation, Phys. Rev. Lett. 53 (17) (1984) 1653–1656.
[15] R. Botet, R. Jullien, Size distribution of clusters in irreversible kinetic aggregation, J. Phys. A Math. Gen. 17 (1984) 2517–2530.
[16] A. Videcoqa, M. Han, P. Abelard, C. Pagnoux, F. Rossignol, R. Ferrando, Influence of the potential range on the aggregation of colloidal particles, Phys. A 374 (2007) 507–516.
[17] M.Yu. Koroleva, A.M. Tokarev, E.V. Yurtov, Langevin-dynamics simulation of flocculation in water-in-oil emulsions, Colloid J. 75 (6) (2013) 660–667.
[18] N. Fuchs, Über die Stabilität und Aufladung der Aerosole, Z. Physik. 89 (11-12) (1934) 736–743.
[19] D.N.L. McGown, C.D. Parfitt, Improved theoretical calculation of the stability ratio for colloidal systems, J. Phys. Chem. 71 (2) (1967) 449–450.
[20] G. Urbina-Villalba, An algorithm for emulsion stability simulations: account of flocculation, coalescence, surfactant adsorption and the process of Ostwald ripening, Int. J. Mol. Sci. 10 (3) (2009) 761–804.
[21] D. Prieve, E. Ruckenstein, Role of surface chemistry in primary and secondary coagulation and heterocoagulation, J. Colloids Interface Sci. 73 (2) (1980) 539–555.
[22] A.K. Atmuri, M.A. Henson, S.R. Bhatia, A population balance equation model to predict regimes of controlled nanoparticle aggregation, Colloids Surfaces A Physicochem. Eng. Aspects 436 (2013) 325–332.
[23] H.A. Kramers, Brownian motion in a field of force and the diffusion model of chemical reactions, Physica 7 (4) (1940) 284–304.
[24] T. Schneider, E. Stoll, Molecular-dynamics study of a three-dimensional one-component model for distortive phase transitions, PRB 17 (3) (1978) 1302–1322.
[25] D. Van Der Spoel, E. Lindahl, B. Hess, G. Groenhof, A.E. Mark, H.J. Berendsen, GROMACS: fast, flexible, and free, J. Comput. Chem. 26 (16) (2005) 1701–1718.
[26] Z. Peng, E. Doroodchi, G. Evans, DEM simulation of aggregation of suspended nanoparticles, Powder Technol. 204 (2010) 91–102.
[27] M.Yu. Koroleva, E.V. Yurtov, I.O. Leoshkevich, Flocculation of dispersed phase droplets in water-in-oil emulsions: experiment and mathematical simulation, Colloid J. 73 (1) (2011) 65–71.
[28] D.A. Turchenkov, M.A. Turchenkov, Analysis of simplifications of numerical schemes for Langevin equation, effect of variations in the correlation of augmentations, Comput. Res. Model. 4 (2) (2012) 325–338 [In Russian].
[29] M. Koroleva, A. Tokarev, E. Yurtov, Simulation of flocculation in W/O emulsions and experimental study, Colloids Surfaces A Physicochem. Eng. Aspects 481 (2015) 237–243.
[30] GROMACS Documentation. Release, GROMACS Development Team. Dec 31, 2018, 2019, p. 333. http://manual.gromacs.org/.
[31] A.P. Babichev, N.A. Babushkina, A.M. Bratkovskii, et al., Physical Quantities, Handbook, Energoatomizdat, Moscow, 1991 [in Russian].
[32] G.Sh. Boltachev, M.G. Ivanov, S.A. Risovaniy, E.A. Chingina, Concentrated nanoparticle suspension: 2D simulations by stochastic dynamics, in: XLVII International Conference "Advanced Problems in Mechanics", APM 2019 Book of Abstracts, June 24-29, 2019, Polytechnic University, St. Petersburg, Peter the Great St. Petersburg, 2019, 10–10.
[33] H.C. Hamaker, The London – van der Waals attraction between spherical particles, Physica 4 (10) (1937) 1058–1072.
[34] G.Sh. Boltachev, N.B. Volkov, Simulation of nanopowder compaction in terms of granular dynamics, Tech. Phys. 56 (7) (2011) 919–930.
[35] G.Sh. Boltachev, N.B. Volkov, K.A. Nagayev, Effect of retardation in the dispersion forces between spherical particles, J. Colloid Interface Sci. 355 (2) (2011) 417–422.
[36] R. Hogg, T.W. Healy, D.W. Fuerstenau, Mutual coagulation of colloidal dispersions, Trans. Faraday Soc. 62 (1966) 1638–1651.
[37] B.V. Deryaguin, N.V. Churaev, V.M. Muller, Surface Forces, Consultants Bureau, Plenum Press, New York, 1987.
[38] I.S. Puzyrev, M.G. Ivanov, I.V. Krutikova, Physicochemical properties of Al_2O_3 and Y_2O_3 nanopowders produced by laser synthesis and their aqueous dispersions, Russ. Chem. Bull. Int. Ed. (Publ. Russ. *Izvestiya Akademii Nauk. Seriya Khimicheskaya*) 63 (7) (2014) 1504–1510.
[39] M.G. Ivanov, Yu.L. Kopylov, V.B. Kravchenko, K.V. Lopukhin, V.V. Shemet, YAG and Y2O3 laser ceramics from nonagglomerated nanopowders, Inorg. Mater. 50 (9) (2014) 951–959.
[40] M. Ivanov, E. Kalinina, Yu. Kopylov, V. Kravchenko, I. Krutikova, U. Kynast, J. Li, M. Leznina, A. Medvedev, Highly transparent Yb-doped $(La_xY_{1-x})_2O_3$ ceramics prepared through colloidal methods of nanoparticles compaction, J. Eur. Ceram. Soc. 36 (2016) 4251–4259.
[41] M.G. Ivanov, I.V. Krutikova, U. Kynast, M. Lezhnina, I.S. Puzyrev, Laser-synthesized Y_2O_3:Eu^{3+} nanophosphors and their stabilization in water suspensions, Opt. Mater. 74 (2017) 67–75.